NeuroImage: Clinical 20 (2018) 705–714

Contents lists available at ScienceDirect

NeuroImage: Clinical

journal homepage: www.elsevier.com/locate/ynicl

Intravoxel incoherent motion MRI in neurological and cerebrovascular diseases☆

André M. Paschoal[a], Renata F. Leoni[a], Antonio C. dos Santos[b], Fernando F. Paiva[c,*]

[a] Inbrain Lab, Department de Física, FFCLRP, Universidade de São Paulo, São Carlos, SP, Brazil
[b] Departamento de Clínica Médica, FMRP, Universidade de São Paulo, São Carlos, SP, Brazil
[c] Instituto de Física de São Carlos, Universidade de São Paulo, São Carlos, SP, Brazil

ABSTRACT

Intravoxel Incoherent Motion (IVIM) is a recently rediscovered noninvasive magnetic resonance imaging (MRI) method based on diffusion-weighted imaging. It enables the separation of the intravoxel signal into diffusion due to Brownian motion and perfusion-related contributions and provides important information on microperfusion in the tissue and therefore it is a promising tool for applications in neurological and neurovascular diseases. This review focuses on the basic principles and outputs of IVIM and details it major applications in the brain, such as stroke, tumor, and cerebral small vessel disease. A bi-exponential model that considers two different compartments, namely capillaries, and medium-sized vessels, has been frequently used for the description of the IVIM signal and may be important in those clinical applications cited before. Moreover, the combination of IVIM and arterial spin labeling MRI enables the estimation of water permeability across the blood-brain barrier (BBB), suggesting a potential imaging biomarker for disrupted-BBB diseases.

1. Introduction

Perfusion refers to the passage of blood delivering nutrients and oxygen to the tissue in the capillary bed (Krogh, 1922). It is an important mechanism of the brain metabolism and plays a crucial role in its normal operation. It is directly involved with regulatory mechanisms (e.g. autoregulation of blood flow, vascular reactivity, and hyperemia) that once unregulated result in cerebral disorders (Hall and Guyton, 2011), such as stroke, dementia and cognitive deficits.

In the brain, perfusion is classically quantified as cerebral blood flow (CBF) which consists of blood volume per unit of brain tissue per unit of time, usually given in mL/100 g/min (Le Bihan, 1992). However, other metrics can be estimated depending on the imaging method. Among several methods, intravoxel incoherent motion (IVIM) estimates brain perfusion based on magnetic resonance imaging (MRI) (Le Bihan et al., 1986). Other approaches are also based on MRI, nuclear medicine and optics (Obrig, 2014; Wintermark et al., 2005).

MRI-based perfusion methods include dynamic contrast enhancement (DCE), dynamic susceptibility contrast (DSC), arterial spin labeling (ASL) (Wintermark et al., 2005), and IVIM. The former two techniques are based on the concept of a bolus of blood volume transiting through the tissue. DCE provides information about K_{trans} (volumetric transfer constant between blood plasma and extracellular extravascular space (EES)) (Sourbron and Buckley, 2013b), permeability-surface area product, and cerebral blood volume (CBV) (Heye et al., 2016; Paldino and Barboriak, 2009). However, the latter is not usually assessed. DSC, the best choice for brain evaluation in clinical settings, provides a relative measurement of CBV, mean transit time (MTT), time to peak (TTP) and an estimation of CBF. ASL is a noninvasive alternative that assesses perfusion through quantification of CBF, which takes advantage of the hydrogen in the arterial blood as an endogenous tracer (Detre et al., 1992; Ferre et al., 2013; Williams et al., 1992).

In the late 1980's, Le Bihan designed IVIM, another approach that measures perfusion-related parameters using MRI noninvasively (Le Bihan et al., 1986). Multiple diffusion-weighted images (DWI) were acquired varying the diffusion gradient weighting. The amplitude of the resulted signal decays exponentially as the diffusion weighting increases. This decay is fitted to a theoretical model to separate diffusion and perfusion contributions of the signal (Le Bihan et al., 1988). A detailed explanation is provided is section 2.

Initially, IVIM drew interest for applications in liver and kidney. Several studies proved its usefulness (Hu et al., 2017; Li et al., 2017; Luciani et al., 2008; Meeus et al., 2018; Yamada et al., 1999). Despite having been initially tested for cerebral imaging, due to its high fractional anisotropy, the existence of several other established imaging methods, and the lack of a consensus about the best fitting method to adjust the signal to a physiological model, IVIM was not very well explored a priori. However, a better physiological description of IVIM

☆ Grant Support: This work was supported by São Paulo Research Foundation (FAPESP) (grant # 2013/23740-0) and National Council for Scientific and Technological Development (CNPq) (grant # 140110/2016-0).

* Corresponding author at: Instituto de Física de São Carlos, Universidade de São Paulo, CP 369, 13560-970, São Carlos, SP, Brazil.
E-mail address: fernando.paiva@usp.br (F.F. Paiva).

https://doi.org/10.1016/j.nicl.2018.08.030
Received 28 March 2018; Received in revised form 27 August 2018; Accepted 30 August 2018
Available online 31 August 2018

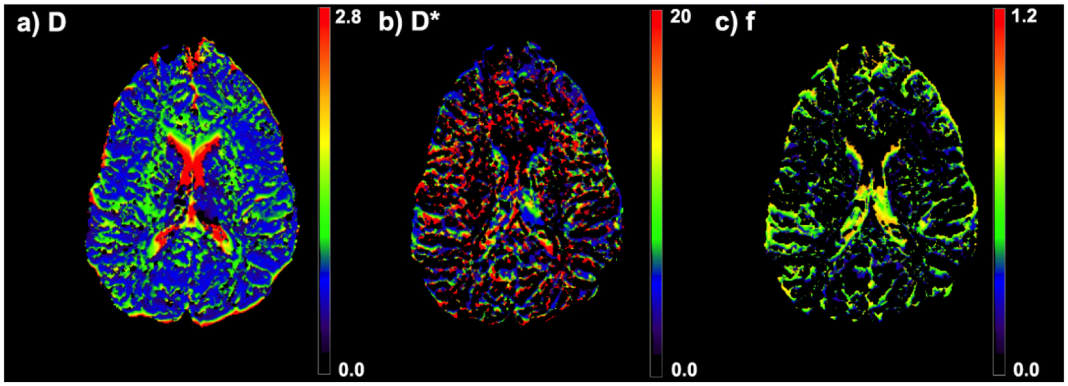

Fig. 1. Examples of D, f and D* maps.

signal and emergence of optimized fitting approaches have increased the application of IVIM in the brain over the past years.

This review provides an overview of the IVIM technique and addresses its main applications in the brain and future directions regarding its use for the study and evaluation of neurological and neurovascular diseases. The combination of IVIM with ASL and their complementarity are also discussed.

2. Theoretical considerations

2.1. The concept of the IVIM signal

Water molecules in a fluid exhibit microscopic random translational motion, called Brownian motion (Einstein, 1956), which results in molecular diffusion. The mean square distance traveled by a molecule is proportional to time and diffusion coefficient D. The latter coefficient depends on diffusing molecules, fluid viscosity, and temperature. At the capillary bed, besides the free water diffusion, the water molecules also flow (Budinger et al., 1985), due to the blood flow. Therefore, in the vascular compartment, the molecular diffusion path is limited by the vessel wall and influenced by the fluid viscosity and blood flow, which results in another diffusion contribution, modulated by a different coefficient, D*, one order of magnitude greater than coefficient D and first described by Le Bihan in 1986 (Le Bihan et al., 1986).

Restrictions imposed on diffusion motion (Tanner and Stejskal, 1968) are measured by MR experiments through the application of magnetic field gradients and result in diffusion-weighted images (Carr and Purcell, 1954; Hahn, 1950). After the use of those gradients, the MR signal decays exponentially according to the diffusion coefficient and the b-value, introduced by Stejskal and Tanner in 1965 (Stejskal and Tanner, 1965) and refers to the weighting of the diffusion pulse sequence. The b-value, expressed in s/mm^2, depends on the diffusion gradient waveform, the time duration of the gradients and the interval between them, according to the following equations:

$$b = (2\pi)^2 \int_0^{TE} \overrightarrow{K_{(t)}} * \overrightarrow{K_{(t)}} dt \tag{1}$$

$$\overrightarrow{K_{(t)}} = \frac{\gamma}{2\pi} \int_0^t \vec{G}_{(t')} dt' \tag{2}$$

where γ is the gyromagnetic ratio, G is the diffusion gradient magnitude in mT/m and t is the time duration of the application of the gradient pulse.

If the signal is measured in a pure solution, where the only source of motion is Brownian due to thermal diffusion, the MR signal can be expressed by a single exponential equation:

$$\frac{S(b)}{S_0} = e^{-bD} \tag{3}$$

where S(b) represents the signal acquired at a specific b-value and S_0 is the signal with no application of diffusion gradients.

When the signal comes from a biological tissue, some factors reduce the diffusion motion, such that it decays according to a different diffusion coefficient, called apparent diffusion coefficient (ADC) (Le Bihan et al., 1986) which is the sum of contribution of all diffusion coefficients related the resulting motion. Under such a condition, diffusion MR signal can be expressed by:

$$\frac{S(b)}{S_0} = e^{-bADC} \tag{4}$$

which is the representation of the diffusion mono-exponential model.

Several components account for the total ADC under biological conditions. However, in comparison to contributions of thermal diffusion and flowing effects, other sources can be neglected, and the signal can be modeled through a bi-exponential model (Eq. (5)), in which each exponential amplitude depends on the blood volume perfusion fraction (f) in a way the sum of those amplitudes must be one.

$$\frac{S(b)}{S_0} = fe^{-bD^*} + (1-f)e^{-bD} \tag{5}$$

Eq. (5) describes the IVIM signal where D is the diffusion coefficient of free water, D* is the pseudo-diffusion coefficient, f is the perfusion fraction and b is the b-value. The idea beyond the IVIM method is to separate those contributions through the mapping of D, D* and f (Fig. 1). Each map contributes with different information, which, combined, helps the understanding of the water movement. Perfusion fraction f represents the volume of blood flowing into the capillary, whose water movement has the contribution of the blood flow and the diffusion motion within a single voxel. All such motions are summarized into pseudo-diffusion coefficient D*. Thus, with the parameters f and D*, IVIM provides the perfusion contribution to the MR signal. Although D* maps are noisier than the others (Fig. 1b), studies in the literature have shown their utility, as discussed in section 2.1. The omission of D* maps might result in the loss of useful information. On the other hand, D is the pure water diffusion coefficient and represents a voxel diffusion contribution to the signal in the extra-vascular pool.

Since D* is one order of magnitude higher than D, the exponential decay with the pseudo-diffusion coefficient vanishes faster, and its contribution to the total signal is distinguishable only at low b-values. At higher b-values, the contribution of the exponential with D models the signal. Multiple b-values are necessary to estimate from which b-value there is only diffusion contribution and consequently to estimate D, D* and f precisely (Fig. 2). Le Bihan proposed acquisition with only three b-values, which are theoretically enough for the obtaining of IVIM outputs. However, more points are necessary especially for the brain due to noise contamination and low D/f ratio, i. e., 0.5%, in comparison to 3.5% in the liver, for example (Le Bihan, 2017). Such a small percentage of perfusion contribution requires oversampling of low b-

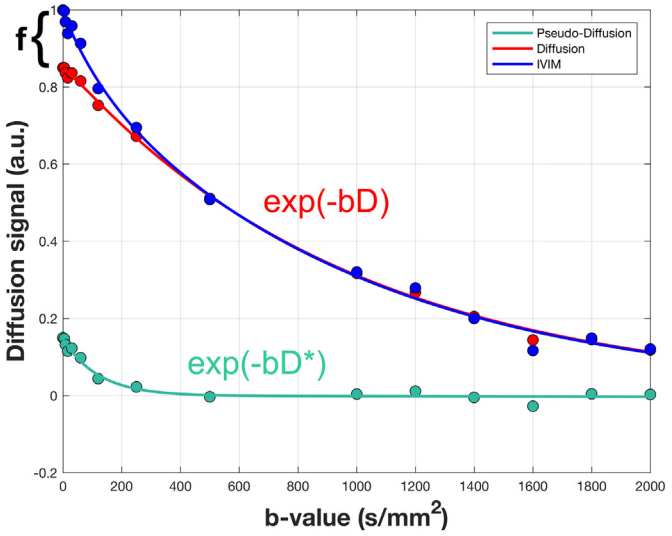

Fig. 2. Example of Pseudo-Diffusion (green) and Diffusion (red) contributions to IVIM signal (blue). Pseudo-diffusion (D*) and diffusion coefficients (D) are extracted from the exponential decay of green and red curves, respectively. Perfusion fraction f is obtained from the difference of the intercept of blue and red curves. (For interpretation of the references to color in this figure legend, the reader is referred to the online version of this chapter.)

values. Therefore, between 10 and 30 b-values are usually employed, and the maximum b-value ranges from 1000 to 2000 s/mm^2 (Lemke et al., 2011).

The IVIM signal represents approximately 5% of the total diffusion signal, which motivated Neil et al. to develop strategies for suppressing the diffusion contribution and better understanding the IVIM signal (Neil et al., 1991). The approach used was the injection of a contrast agent for decreasing T1 and selectively suppressing the signal of non-flowing components. Once the diffusion contribution had been suppressed, the authors expected to fit the resulted signal by a mono-exponential model. However, they observed the signal was better adjusted through a bi-exponential approach. Other studies also investigated that behavior towards explaining the results (Henkelman et al., 1994; Neil and Ackerman, 1992; Neil et al., 1994).

Fournet et al. described a more specific bi-exponential model (Fournet et al., 2017) that considers two different compartments, namely capillaries, and medium-sized vessels. The authors hypothesized the bi-exponential behavior reflected the contribution of flow through two different vascular pools. The slow and fast pools represent capillaries and medium-sized vessels, respectively. That differs from classical IVIM models that consider a single compartment: the intravascular. At high b-values, both models converge to the mono-exponential decay, however, at low b-values, the signal is better fitted considering two pools. Such information helps the understanding of the IVIM signal and can also be useful for clinical applications.

2.2. Physiological models and fitting approaches

Since IVIM was proposed in 1986, several models were developed to explain the physiology related to the IVIM signal (physiological models) and others to fit better the acquired signal resulting in more trustful output maps (fitting models/approaches). However, there is some confusion in the literature about the terminology employed to classify all these models, especially about the bi-exponential terminology that is recurrently used to refer to both physiological and fitting models.

2.2.1. Physiological models

Physiological models aim to explain the nature of the measured IVIM signal. Le Bihan et al. (1988) introduced the two first models, the mono-exponential and sinc models. Part of the confusion on terminology is related to the mono-exponential model since it is described by an equation of two exponential terms (Eq. (5)). It is referred to as mono-exponential because only one compartment (the intravascular one) is used for explaining the pseudo-diffusion contribution to a single exponential term. On the other hand, Fournet's bi-exponential IVIM model considers two compartments, namely capillaries and medium-sized vessels, to explain the pseudo-diffusion and perfusion related information (Fournet et al., 2017). Therefore, the use of mono- and bi-compartment models may help to end the confusion.

2.2.2. Fitting models

The main step of the IVIM data analysis consists of fitting the measured signal to a theoretical model and, consequently, researches have focused on the optimization of the fitting approaches. Classically, the IVIM signal is fitted through a two-step mono-exponential analysis. First, the diffusion coefficient (D) is obtained from the mono-exponential fitting of the exponential decay for high b-values (usually higher than 200 s/mm^2). Then, a mono-exponential fitting of the exponential decay for low b-values is applied towards estimating the pseudo-diffusion coefficient (D*) and perfusion fraction (f). The other usual fitting model is the bi-exponential, which tries to adjust the entire curve including all b-values to obtain D, D* and f. The approach is commonly used for the mono-exponential physiological model.

Several studies have implemented more robust models for fitting the IVIM signal, e.g. kurtosis model, non-negative least squares (NNLS), models that use artificial neural network and Bayesian approaches. Details can be found in (Bertleff et al., 2017; Gustafsson et al., 2018; Keil et al., 2017).

2.3. IVIM and classical perfusion measurements

IVIM emerged as a different approach for the obtaining of perfusion information and studies have aimed to correlate IVIM outputs with standard perfusion-related measures, as CBF and CBV (Bisdas et al., 2014; Henkelman, 1990; Le Bihan and Turner, 1992).

Conventional perfusion can be assessed by nuclear medicine techniques, as positron emission tomography (PET) and single photon emission computed tomography (SPECT). In both techniques, a bolus of exogenous tracer is intravenously injected for tagging the arterial blood with radioisotopes. Emissions from radioisotopes enable the estimation of the delivery of nutrients, as oxygen, glucose and tracer injected in the tissues, which results in the measurement of CBF in physiological units, mL/100 g of tissue/min (Le Bihan, 1992).

MRI-based DSC and DCE are well established methods applied in clinical routine for the assessment of perfusion (Sourbron and Buckley, 2013a). DSC uses T2*-weighted images of high temporal resolution to calculate perfusion-related metrics (CBV, MTT and TTP), towards CBF estimation. On the other hand, DCE – originally a technique to assess permeability of blood-brain barrier (BBB) – estimates CBF and CBV according to dynamic T1-weighted images and classic permeability parameters, as volume transfer constant (K_{trans}) and plasma volume (V_p). It is the best option for the study of neck, breast, and abdomen, which are regions of high field inhomogeneities due to fat, bone and air interfaces that suffer from susceptibility artifacts in T2*-weighted images. However, both methods require an intravenous injection of gadolinium. Besides concerns regarding its deposition in the brain, some factors hamper the quantification of perfusion-related parameters – e.g. gauge of the venous access that limits injection velocity; physical characteristics of the contrast agent, as temperature and viscosity; characteristics of the injection bomb; the injection protocol, and characteristics of patients, as arterial blood pressure and atherosclerosis.

In ASL, labeled blood flows through capillaries, delivers nutrients and oxygen to the brain tissue, and exchanges magnetization. The approach consists in the magnetic labeling of the arterial blood through the application of radiofrequency pulses. After the labeled blood has

reached the slices of interest, the image is acquired and then subtracted from a label-free image acquired at the same position, which results in a perfusion map proportional to the CBF (Buxton, 2005; Buxton et al., 1998) that takes into account some physiological and acquisition parameters (Alsop et al., 2015).

On the other hand, IVIM perfusion measures all water motion contributions to the intravoxel signal, as the Brownian motion of free water at perivascular space, the microperfusion signal of water flowing in randomly distributed microvasculature and flowing blood inside arteries. Since f represents the volume fraction of the intravascular blood and D* refers to pseudo-diffusion motions related to blood flow, these measurements can be connected to those of classical methods. The first hypothesis proposed by Le Bihan and colleagues (Le Bihan, 2017; Le bihan and Turner, 1992) suggests the link is related to capillary network geometry, as described by:

$$f_{IVIM} = \frac{CBV}{f_w} \tag{6}$$

$$MTT = \frac{L}{v} = \frac{Ll}{6D^*} \tag{7}$$

$$CBF = \left(\frac{6f_w}{Ll}\right) f_{IVIM} D^* \tag{8}$$

where f_w is the MRI-visible water content fraction, L is the total capillary length, l is the mean capillary segment length and v is the average blood velocity. Therefore, CBF is related to IVIM perfusion through product fD*.

Recent studies have compared the blood flow measured with ASL and fD* measured with IVIM. Yao and colleagues showed the correlation between fD* and ASL-CBF was fair to good for stroke patients (Yao et al., 2016). Liang and colleagues also obtained a good correlation with the renal cortex, but weak correlation when the whole kidney was considered (Liang et al., 2016). Wu and colleagues did not achieve the same good correlation for the brain (Wu et al., 2015). Therefore, the comparison between IVIM parameters and ASL-CBF is still inconclusive and must be clarified. However, more than comparing IVIM parameters with standard ones, it is important to understand their physiological meaning, since they may provide complementary and useful information.

3. Neurological and Neurovascular applications

The analysis of neurological and neurovascular diseases revealed that measures of perfusion provide essential information for the patient's diagnosis and the disease characterization and monitoring. IVIM is an imaging tool that represents a new insight in perfusion measurements combined with simultaneously acquired diffusion information. Since its development, some applications for IVIM such as glioma grading, tumor diagnosis, stroke and cerebral death have been reported (Federau et al., 2014b), and once the results have proven positive, their range has been extended over the past few years.

3.1. Cerebrovascular diseases

3.1.1. Stroke

Stroke is the second leading cause of death worldwide (World Health Organization, 2017), therefore, it has been the subject of extensive studies regarding its characterization, diagnosis, and tissue lesion progression. Besides structural sequences, as T2W, T1W and T2-FLAIR (fluid attenuation inversion recovery), the standard protocols used for stroke evaluation include DWI and perfusion-weighted imaging. The current perfusion mapping is mostly performed by DSC, DCE and, more recently ASL methods (Heye et al., 2014; Huang et al., 2013; Zhang et al., 2015). Measurements of perfusion in stroke aim to assess the reduction of regional blood flow, volume and transit time through maps of CBF, CBV, and MTT, respectively. However, DSC and DCE use gadolinium-based contrast injected in peripheral veins and are highly dependent on hemodynamics impairment, stenosis of proximal large arteries and velocity of contrast injection. Moreover, they provide information mainly from large vessels rather than the microvasculature (Jahng et al., 2014). On the other hand, the use of ASL, the classic non-contrast-agent technique, strongly depends on changes in the arterial arrival time and may provide underestimated CBF values (MacIntosh et al., 2010).

IVIM provides intrinsically local information, and nondependent on the regional effects of big arteries and peripheral hemodynamic impairment or problems related to gadolinium injection. It also provides absolute perfusion and diffusion information with a single three-minute sequence. According to IVIM-based maps, information from D or ADC enables the anatomical determination of stroke lesions since it indicates the degree of diffusion restriction of water molecules (Muir et al., 2006). Simultaneously, due to incoherent motion, perfusion information is also available (f map) making it possible to determine if it is from intra- or extravascular medium.

The assessment of stroke by IVIM was first reported by Wirestam et al. (Wirestam et al., 1997). Perfusion fraction f was reduced in affected areas in comparison to the respective contralateral region. After that study, stroke evaluation by IVIM was not reported until 2014, when Federau et al. revisited (Federau et al., 2014c). In agreement with the previous study (Wirestam et al., 1997), the authors also reported a reduction in perfusion fraction f in 14 out of 17 patients. The novelty was the combined analysis of quantitative maps of ADC and f (Fig. 3b and c), which provided information about the penumbra region.

Other studies reported the possible use of different IVIM outputs, as maps of D, ADC, D*, f, and fD* for analysis of affected regions (Hu et al., 2015; Yao et al., 2016). The authors concluded f and fD* are more sensitive to detect changes during the stroke process, as these parameters are more related to CBF, with similar results to those obtained using ASL. In a different analysis, Suo et al. evaluated the correlation between ADC and IVIM-derived parameters and showed that for stroke lesions this correlation is different in comparison to normal tissue. Such a difference is clear in the analysis of the scatter plot of the correlations, where stroke areas can be distinguished, especially for the ADC-f correlation (Suo et al., 2016).

3.1.2. Cerebral small vessel disease

A novel application of IVIM refers to the assessment of patients with cerebral small vessel disease (CSVD), a common microvascular pathology that can progress to complications such as lacunar stroke, leukoaraiosis and vascular dementia (Wardlaw, 2010; Wardlaw et al., 2013a). Such patients have reported alterations in the parenchyma, lacunes, enlarged perivascular spaces (PVS) and atrophy, which result in structural MRI abnormalities, as hyperintensities and microbleeds (Cordonnier et al., 2007; Ewers et al., 2006; Jovicich et al., 2009; Kruggel et al., 2010; Reig et al., 2009; Roob et al., 1999; Schnack et al., 2004; Wardlaw et al., 2013c; Wonderlick et al., 2009). Although the identification of CSVD through conventional MRI is relatively easy, finding indications of normal appearing white matter (NAWM) that can advance to CSVD is still a challenge.

Perfusion images have shown a reduction in white matter CBF for CSVD patients (Markus et al., 2000; O'Sullivan et al., 2002), while DWI has also shown abnormalities (Wardlaw et al., 2013b).

Wong et al. used FLAIR image to localize affected areas (Fig. 4a) and IVIM to estimate perfusion fraction f (Fig. 4b) (Wong et al., 2017). They observed an increase in f values for both affected areas and in regions of FLAIR-NAWM, which is contrary to previous perfusion-based studies in CSVD. The results may be an evidence of vasodilation to increase the blood flow in those regions to suppress the cognition loss effects. Other possible explanations include deregulation in blood-brain barrier (BBB) and effects of increased vessel tortuosity. Even though the authors showed that IVIM might be useful to indicate affected regions before

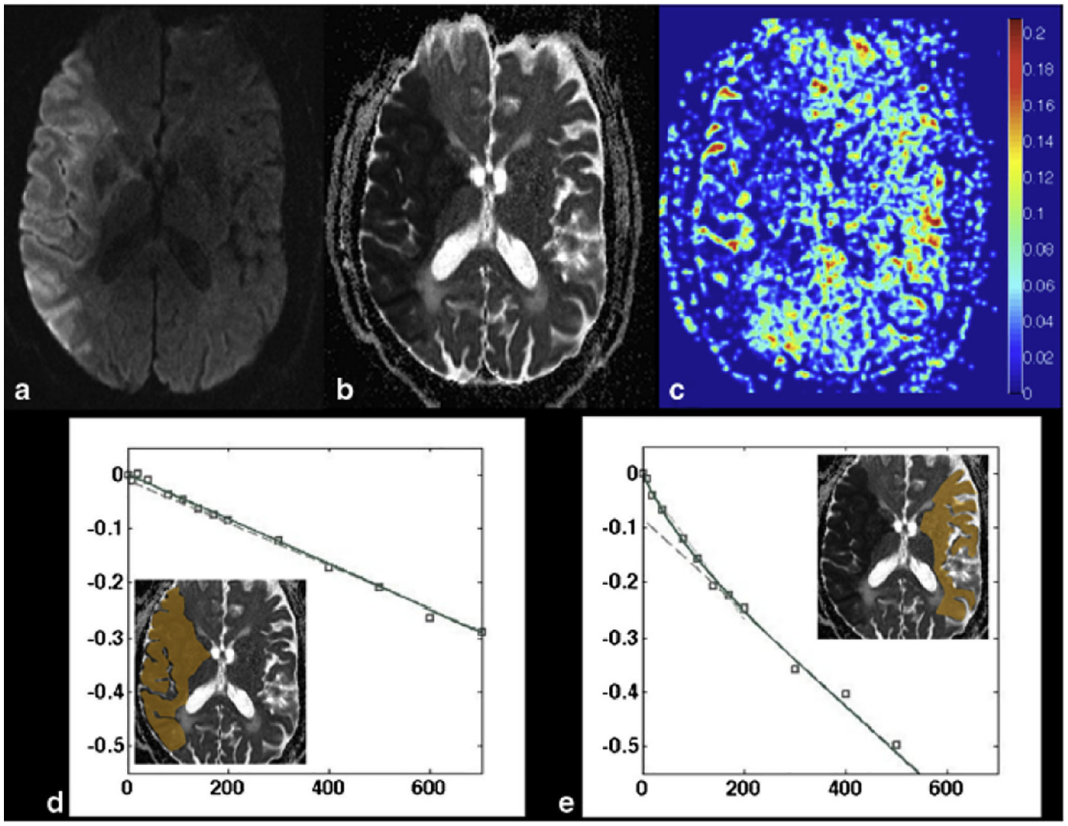

Fig. 3. Example of a patient with a stroke in the middle cerebral artery territory. a) Raw image (b = 900 s/mm^2). b) ADC map. c) Perfusion fraction map. d) IVIM fitting in the stroke area. e) IVIM fitting in the contralateral hemisphere (Federau et al., 2014c).

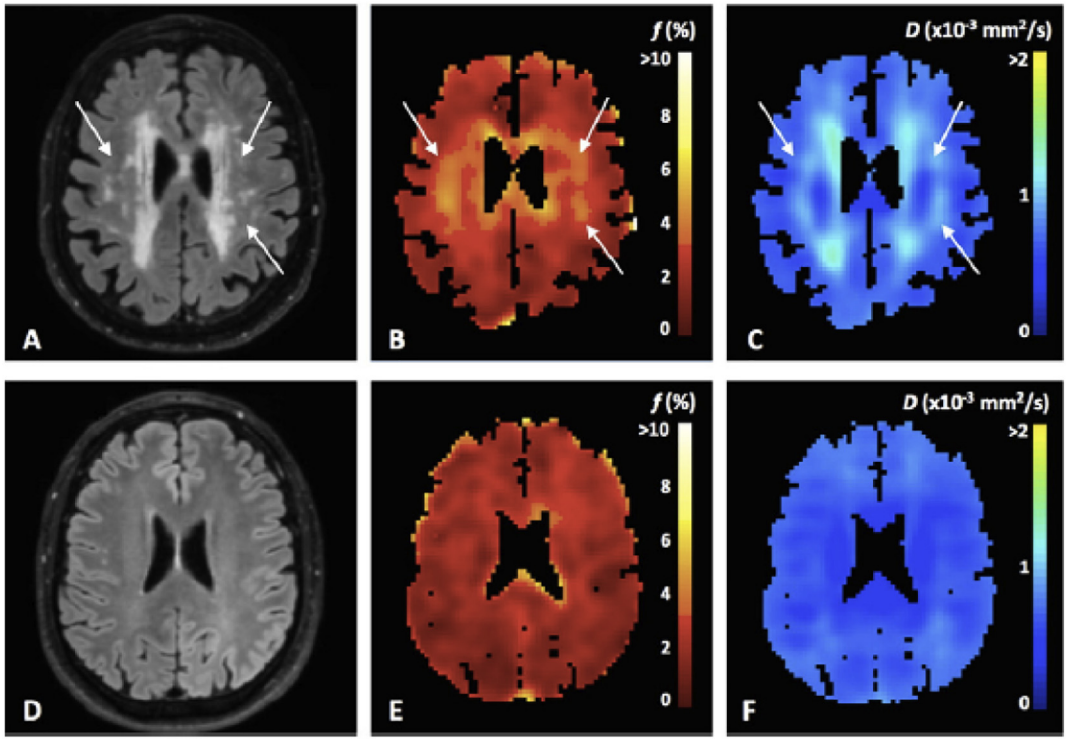

Fig. 4. Example of FLAIR images (A, D), perfusion fraction f maps (B, E) and parenchymal diffusivity D (C, F) for a small vessel disease patient (top row) and a healthy subject (bottom row) (Wong et al., 2017).

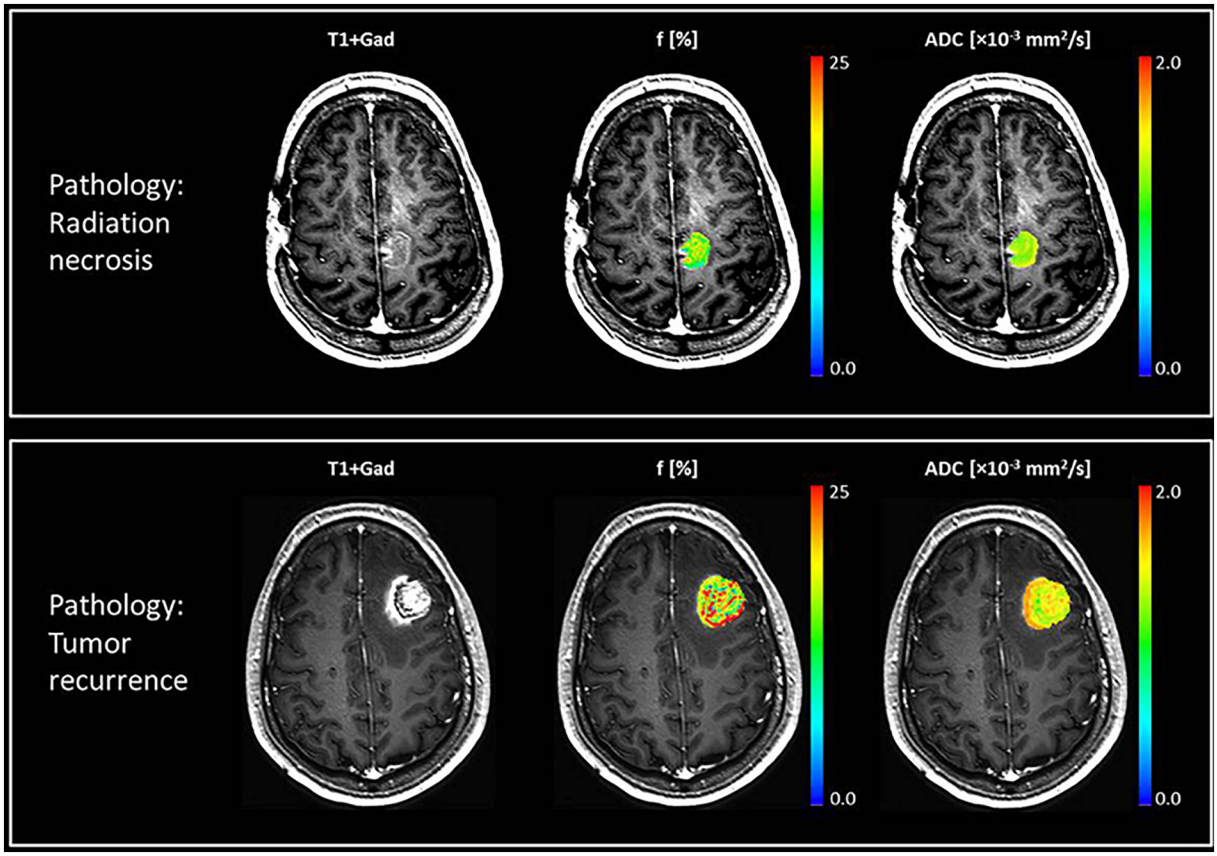

Fig. 5. Example of IVIM parameter maps for a patient with radiation necrosis (top row) and another with tumor recurrence (bottom row) (Detsky et al., 2017).

structural MRI, future studies must investigate the mechanism more carefully.

3.2. Tumor

Brain tumors deriving from cells of the central nervous system (CNS) are classified into benign and malignant. The most common malignant brain tumors are diffuse gliomas, mainly astrocytomas, and glioblastomas (de Robles et al., 2015). Due to their high mortality rate, early diagnosis and precise characterization are crucial to the treatment prospectus. Clinically, DSC and DWI are commonly used to help the diagnosis in case of tumor suspicion (Mullen and Huang, 2017). Therefore, tumors have quickly become an important target of application for IVIM that provides perfusion and diffusion information (Federau et al., 2014b).

3.2.1. Glioma

Glial tumors represent over 50% of primary brain neoplasms and approximately 80% of all malignant brain tumors (Goodenberger and Jenkins, 2012). Term glioma refers to all glial tumors, however diffuse gliomas (grades II to IV) are more critical than low proliferative and well-delimitated gliomas (grade I), which enable complete surgical resection. Diffuse gliomas are divided into low grade (LGG, grade II), high grade (HGG, grade III), and glioblastoma (GBM, grade IV), according to the World Health Organization (WHO) (Louis et al., 2016). Histologically, grade II gliomas have well-differentiated cells, and patients have an average survival of 5 to 10 years after diagnosis. Grade III anaplastic oligodendrogliomas or astrocytomas show anaplasia and mitotic activity and patients usually survive less than 5 years. Grade IV GBM shows further microvascular proliferation and necrosis and is associated with less than two-year average survival. Because of such differences, therapeutic strategies are different, and the grading of diffuse gliomas is crucial.

Bisdas showed the first evidence that IVIM could provide useful information in grading gliomas (Bisdas et al., 2013). They reported both D^* and f could be used to differentiate gliomas since these parameters were higher in HGG in comparison to LGG, which is consistent with the pathophysiology of the disease. Other researchers have reported similar results and emphasized IVIM-derived parameters could be used as markers for the diagnosis of glioma (Federau et al., 2014a; Togao et al., 2016).

According to Hu et al. ADC and D were significantly lower in HGG in comparison to LGG and, similarly to previous studies, D* at tumor site showed higher values for HGG (Hu et al., 2014). However, the authors found lower f values for HGG, possibly due to the use of different b-values, especially for lower ones, and to ROI selection that, in contrast to other studies, included the solid tumor with the highest signal intensity on DWI. Moreover, the highest cellularity density, nuclear-cytoplasmic ratio, and relatively fewer mesenchymal components are present in anaplastic gliomas and glioblastomas (Plate et al., 1992), which are possible sources of reduction in perfusion fraction (Bisdas et al., 2013; Federau et al., 2014a).

There are also reports on IVIM to differentiate between glioblastoma, metastasis and primary central nervous system lymphoma (PCNSL) (Shim et al., 2015; Suh et al., 2014; Yamashita et al., 2016). Other researchers reported ADC obtained from a mono-exponential model of DWI could differentiate glioblastoma from PCNSL (Calli et al., 2006; Guo et al., 2002; Toh et al., 2008; Yamasaki et al., 2005). However, there is evidence that perfusion effects enhance this difference in ADC within the affected region. Suh et al. used the bi-exponential model to separate perfusion and diffusion information on the IVIM signal and found no significant difference in the D coefficient comparing PNCSL and glioblastoma. They suggested the difference in ADC was related to perfusion (Suh et al., 2014), which was confirmed

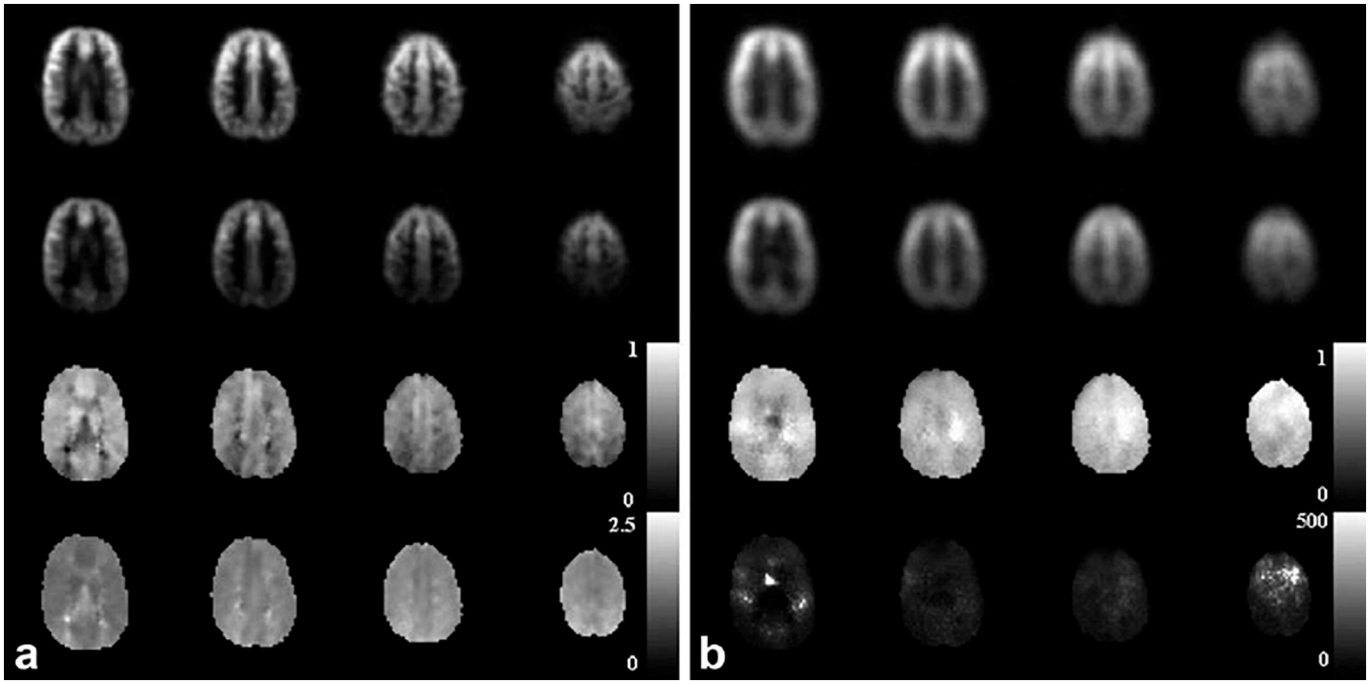

Fig. 6. Examples of ASL-DWI images. For both figures a and b, first row shows the average diffusion-weighted (ΔM) maps for b_0; second row shows ΔM including diffusion weighting (b_{dw}); third row shows the ratio $\Delta M(b_{dw})/\Delta M(b_0)$. In fourth row, in figure a it is shown the Transit time to the capillary-tissue compartment (τ_a) while in figure b it is presented the exchange rate of water from blood to tissue (k_w) (Lawrence et al., 2012)

through the analysis of the perfusion fraction f higher in glioblastoma than in PNCSL, such a result is in agreement with histological examination, once the level of cellularity in tumors is higher in comparison to normal tissue (Guo et al., 2002; Toh et al., 2008; Yamasaki et al., 2005).

3.2.2. *Tumor monitoring*

IVIM parameters have been used in the monitoring of tumors in patients treated with drugs, as antiangiogenic and vascular target agents applied outside the brain (Cui et al., 2015; Joo et al., 2016; Joo et al., 2014; Marzi et al., 2015; Yang et al., 2017).

Detsky and colleagues used IVIM imaging to investigate patients subjected to stereotactic radiotherapy (Detsky et al., 2017), and differentiate radiation necrosis from tumor progression. This differentiation is crucial for the continuation of or changes in the treatment. A signal enhancement in conventional MRI for both tumor progression and radiation necrosis hampers differentiation, although occurring in different scales. Detsky et al. showed perfusion fraction f might be useful for that differentiation (Fig. 5). The perfusion fraction map is uniformly low in the affected region for the radiation necrosis (top row of Fig. 5), whereas for tumor recurrence, it is more heterogeneous and shows higher perfusion fraction values (bottom row of Fig. 5). However, such findings must be validated in a larger cohort.

4. Combination of IVIM and ASL

Recent studies have documented gadolinium deposits in the brain and adverse effects in several subjects (Costa et al., 2018; Fitzgerald et al., 2018; Pullicino et al., 2018; Rahatli et al., 2018). As addressed in section 1, an accurate estimation of perfusion parameters based on DSC and DCE depends on different factors, including injection protocol and patients' anatomical vascularization. Therefore, a combination of ASL and IVIM may render a possible diagnostic benefit without the use of gadolinium.

Early ASL models assumed the labeled arterial blood could be classified as a freely diffusible tracer (Detre et al., 1992). However, other studies have reported the assumption is not completely valid, due to regulatory mechanisms of BBB that reduce water permeability according to the tissue necessity (Eichling et al., 1974; Li et al., 2005; Parkes and Tofts, 2002; Zhou et al., 2001). Researchers started to assess the ASL signal through a two-compartment model that considers BBB permeability. ASL images acquired at multiple inflow times, which is known as multi-TI/PLD ASL, are an alternative for the obtaining of the BBB permeability resulted from a fitting model. However, the origin of ASL signal must be investigated through its splitting into intravascular and extravascular contributions, which can be done with IVIM. Therefore, a combination of ASL and IVIM started to be considered.

The combination of ASL and diffusion gradients was first described by Wang et al. (Wang et al., 2007), who used a hybrid sequence of continuous ASL and the twice-refocused spin-echo method for acquiring images with different b-values at three different post-labeling delays (PLDs). They estimated the BBB permeability to water through the bi-exponential model. Lawrence et al. reported a similar study but using a two-stage approach (Lawrence et al., 2012). First, the hybrid ASL-DWI sequence was used in the estimation of b-values necessary for the separation of extra and intravascular components of the ASL signal. Using only the chosen b-values and varying the PLD, the authors acquired images that enabled the calculation of each contribution to the signal (Fig. 6).

Other studies have aimed at better results of BBB permeability and understanding of the origin of the MRI perfusion signal (Hales and Clark, 2013; Zhang et al., 2018). The results of the combination of ASL and IVIM methods are promising and suggest a possible new imaging tool for the assessment of water exchange across BBB, providing important information about diseases as tumor and CSVD, and neurodegeneration.

5. Conclusions

IVIM method is a diffusion-weighted MRI sequence for the estimation of perfusion parameters that offers several advantages in comparison to commonly used approaches. First, it is a noninvasive alternative for the measurement of perfusion with no intravenous injection of exogenous contrast agents, as gadolinium, and provides information on

perfusion and diffusion simultaneously through a single image sequence, which shortens the exam. Third, its signal has high spatial specificity since it comes primarily from where the measure is achieved independently of the arterial blood path before arriving there. Finally, it provides complementary information in comparison to ASL and the combination of both methods can be useful for the assessment of neurological diseases.

However, for being a recently rediscovered method, especially for brain applications, IVIM is in development in almost every stage, such as acquisition, analysis, and applications. There is still discussion on how many b-values are necessary to obtain a reliable signal fitting, the maximum b-value to be acquired and the cutoff value where diffusion dominates the signal. Regarding analysis, physiological models and fitting strategies are still under investigation.

Conflict of interest

The author(s) declare(s) that there is no conflict of interest regarding the publication of this paper.

Acknowledgments

The authors would like to acknowledge Angela Cristina Pregnolato Giampedro for editing the manuscript for language and style.

References

Alsop, D.C., Detre, J.A., Golay, X., Gunther, M., Hendrikse, J., Hernandez-Garcia, L., Lu, H., MacIntosh, B.J., Parkes, L.M., Smits, M., van Osch, M.J., Wang, D.J., Wong, E.C., Zaharchuk, G., 2015. Recommended implementation of arterial spin-labeled perfusion MRI for clinical applications: a consensus of the ISMRM perfusion study group and the European consortium for ASL in dementia. Magn. Reson. Med. 73, 102–116.

Bertleff, M., Domsch, S., Weingartner, S., Zapp, J., O'Brien, K., Barth, M., Schad, L.R., 2017. Diffusion parameter mapping with the combined intravoxel incoherent motion and kurtosis model using artificial neural networks at 3 T. NMR Biomed. 30.

Bisdas, S., Koh, T.S., Roder, C., Braun, C., Schittenhelm, J., Ernemann, U., Klose, U., 2013. Intravoxel incoherent motion diffusion-weighted MR imaging of gliomas: feasibility of the method and initial results. Neuroradiology 55, 1189–1196.

Bisdas, S., Braun, C., Skardelly, M., Schittenhelm, J., Teo, T.H., Thng, C.H., Klose, U., Koh, T.S., 2014. Correlative assessment of tumor microcirculation using contrast-enhanced perfusion MRI and intravoxel incoherent motion diffusion-weighted MRI: is there a link between them? NMR Biomed. 27, 1184–1191.

Budinger, T.F., Knittel, B.L., Bruner, P., Harrison, C., 1985. Tissue perfusion phantom for magnetic resonance flow studies. In: 4th Annual Meeting of Society of Magnetic Resonance in Medicine, Berkley, California, pp. 577–588.

Buxton, R.B., 2005. Quantifying CBF with arterial spin labeling. J. Magn. Reson. Imaging 22, 723–726.

Buxton, R.B., Frank, L.R., Wong, E.C., Siewert, B., Warach, S., Edelman, R.R., 1998. A general kinetic model for quantitative perfusion imaging with arterial spin labeling. Magn. Reson. Med. 40, 383–396.

Calli, C., Kitis, O., Yunten, N., Yurtseven, T., Islekel, S., Akalin, T., 2006. Perfusion and diffusion MR imaging in enhancing malignant cerebral tumors. Eur. J. Radiol. 58, 394–403.

Carr, H.Y., Purcell, E.M., 1954. Effects of diffusion on free precession in nuclear magnetic resonance experiments. Phys. Rev. 94, 630–638.

Cordonnier, C., Al-Shahi Salman, R., Wardlaw, J., 2007. Spontaneous brain microbleeds: systematic review, subgroup analyses and standards for study design and reporting. Brain 130, 1988–2003.

Costa, A., Ronchi, A., Pigatto, P.D., Guzzi, G., 2018. Brain gadolinium deposition, hyperintense MRI signals, and resonance contrast agents. Magn. Reson. Imaging 137–138.

Cui, Y., Zhang, C., Li, X., Liu, H., Yin, B., Xu, T., Zhang, Y., Wang, D., 2015. Intravoxel incoherent motion diffusion-weighted magnetic resonance imaging for monitoring the early response to ZD6474 from nasopharyngeal carcinoma in Nude Mouse. Sci. Rep. 5, 16389.

de Robles, P., Fiest, K.M., Frolkis, A.D., Pringsheim, T., Atta, C., St Germaine-Smith, C., Day, L., Lam, D., Jette, N., 2015. The worldwide incidence and prevalence of primary brain tumors: a systematic review and meta-analysis. Neuro-Oncology 17, 776–783.

Detre, J.A., Leigh, J.S., Williams, D.S., Koretsky, A.P., 1992. Perfusion imaging. Magn. Reson. Med. 23, 37–45.

Detsky, J.S., Keith, J., Conklin, J., Symons, S., Myrehaug, S., Sahgal, A., Heyn, C.C., Soliman, H., 2017. Differentiating radiation necrosis from tumor progression in brain metastases treated with stereotactic radiotherapy: utility of intravoxel incoherent motion perfusion MRI and correlation with histopathology. J. Neuro-Oncol. 134, 433–441.

Eichling, J.O., Raichle, M.E., Grubb Jr., R.L., Ter-Pogossian, M.M., 1974. Evidence of the limitations of water as a freely diffusible tracer in brain of the rhesus monkey. Circ. Res. 35, 358–364.

Einstein, A., 1956. Investigations on the Theory of the Brownian Movement. Dover Publications, New York.

Ewers, M., Teipel, S.J., Dietrich, O., Schonberg, S.O., Jessen, F., Heun, R., Scheltens, P., van de Pol, L., Freymann, N.R., Moeller, H.J., Hampel, H., 2006. Multicenter assessment of reliability of cranial MRI. Neurobiol. Aging 27, 1051–1059.

Federau, C., Meuli, R., O'Brien, K., Maeder, P., Hagmann, P., 2014a. Perfusion measurement in brain gliomas with intravoxel incoherent motion MRI. Am. J. Neuroradiol. 35, 256–262.

Federau, C., O'Brien, K., Meuli, R., Hagmann, P., Maeder, P., 2014b. Measuring brain perfusion with intravoxel incoherent motion (IVIM): initial clinical experience. J. Magn. Reson. Imaging 39, 624–632.

Federau, C., Sumer, S., Becce, F., Maeder, P., O'Brien, K., Meuli, R., Wintermark, M., 2014c. Intravoxel incoherent motion perfusion imaging in acute stroke: initial clinical experience. Neuroradiology 56, 629–635.

Ferre, J.C., Bannier, E., Raoult, H., Mineura, G., Carsin-Nicol, B., Gauvrit, J.Y., 2013. Arterial spin labeling (ASL) Perfusion: techniques and clinical use. J. De Radiol. Diag. et Intervent. 94, 1208–1221.

Fitzgerald, R.T., Agarwal, V., Hoang, J.K., Gaillard, F., Dixon, A., Kanal, E., 2018. The impact of gadolinium deposition on radiology practice: an international survey of radiologists. Curr. Probl. Diagn. Radiol.

Fournet, G., Li, J.R., Cerjanic, A.M., Sutton, B.P., Ciobanu, L., Le Bihan, D., 2017. A two-pool model to describe the IVIM cerebral perfusion. J. Cereb. Blood Flow Metab. 37, 2987–3000.

Goodenberger, M.L., Jenkins, R.B., 2012. Genetics of adult glioma. Cancer Genet. 205, 613–621.

Guo, A.C., Cummings, T.J., Dash, R.C., Provenzale, J.M., 2002. Lymphomas and high-grade astrocytomas: comparison of water diffusibility and histologic characteristics. Radiology 224, 177–183.

Gustafsson, O., Montelius, M., Starck, G., Ljungberg, M., 2018. Impact of prior distributions and central tendency measures on Bayesian intravoxel incoherent motion model fitting. Magn. Reson. Med. 79, 1674–1683.

Hahn, E.L., 1950. Spin Echoes. Phys. Rev. 77, 746.

Hales, P.W., Clark, C.A., 2013. Combined arterial spin labeling and diffusion-weighted imaging for noninvasive estimation of capillary volume fraction and permeability-surface product in the human brain. J. Cereb. Blood Flow Metab. 33, 67–75.

Hall, J.E., Guyton, A.C., 2011. Guyton and Hall Textbook of Medical Physiology, 12th ed. Saunders/Elsevier, Philadelphia, PA.

Henkelman, R.M., 1990. Does Ivim measure Classical Perfusion. Magn. Reson. Med. 16, 470–475.

Henkelman, R.M., Neil, J.J., Xiang, Q.S., 1994. A quantitative interpretation of Ivim measurements of vascular perfusion in the rat-brain. Magn. Reson. Med. 32, 464–469.

Heye, A.K., Culling, R.D., Valdes Hernandez Mdel, C., Thrippleton, M.J., Wardlaw, J.M., 2014. Assessment of blood-brain barrier disruption using dynamic contrast-enhanced MRI. A systematic review. Neuroimage Clin. 6, 262–274.

Heye, A.K., Thrippleton, M.J., Armitage, P.A., Valdes Hernandez, M.D.C., Makin, S.D., Glatz, A., Sakka, E., Wardlaw, J.M., 2016. Tracer kinetic modelling for DCE-MRI quantification of subtle blood-brain barrier permeability. NeuroImage 125, 446–455.

Hu, Y.C., Yan, L.F., Wu, L., Du, P., Chen, B.Y., Wang, L., Wang, S.M., Han, Y., Tian, Q., Yu, Y., Xu, T.Y., Wang, W., Cui, G.B., 2014. Intravoxel incoherent motion diffusion-weighted MR imaging of gliomas: efficacy in preoperative grading. Sci. Rep. 4.

Hu, L.B., Hong, N., Zhu, W.Z., 2015. Quantitative measurement of cerebral perfusion with intravoxel incoherent motion in acute ischemia stroke: initial clinical experience. Chin. Med. J. 128, 2565–2569.

Hu, F., Yang, R., Huang, Z., Wang, M., Zhang, H., Yan, X., Song, B., 2017. Liver fibrosis: in vivo evaluation using intravoxel incoherent motion-derived histogram metrics with histopathologic findings at 3.0 T. Abdom. Radiol. (NY). 42, 2855–2863.

Huang, Y.C., Liu, H.L., Lee, J.D., Yang, J.T., Weng, H.H., Lee, M., Yeh, M.Y., Tsai, Y.H., 2013. Comparison of arterial spin labeling and dynamic susceptibility contrast perfusion MRI in patients with acute stroke. PLoS One 8, e69085.

Jahng, G.H., Li, K.L., Ostergaard, L., Calamante, F., 2014. Perfusion magnetic resonance imaging: a comprehensive update on principles and techniques. Korean J. Radiol. 15, 554–577.

Joo, I., Lee, J.M., Han, J.K., Choi, B.I., 2014. Intravoxel incoherent motion diffusion-weighted MR imaging for monitoring the therapeutic efficacy of the vascular disrupting agent CKD-516 in rabbit VX2 liver tumors. Radiology 272, 417–426.

Joo, I., Lee, J.M., Grimm, R., Han, J.K., Choi, B.I., 2016. Monitoring vascular disrupting therapy in a rabbit liver tumor model: relationship between tumor perfusion parameters at IVIM diffusion-weighted MR imaging and those at dynamic contrast-enhanced MR imaging. Radiology 278, 104–113.

Jovicich, J., Czanner, S., Han, X., Salat, D., van der Kouwe, A., Quinn, B., Pacheco, J., Albert, M., Killiany, R., Blacker, D., Maguire, P., Rosas, D., Makris, N., Gollub, R., Dale, A., Dickerson, B.C., Fischl, B., 2009. MRI-derived measurements of human subcortical, ventricular and intracranial brain volumes: Reliability effects of scan sessions, acquisition sequences, data analyses, scanner upgrade, scanner vendors and field strengths. NeuroImage 46, 177–192.

Keil, V.C., Madler, B., Gielen, G.H., Pintea, B., Hiththetiya, K., Gaspranova, A.R., Gieseke, J., Simon, M., Schild, H.H., Hadizadeh, D.R., 2017. Intravoxel incoherent motion MRI in the brain: Impact of the fitting model on perfusion fraction and lesion differentiability. J. Magn. Reson. Imaging 46, 1187–1199.

Krogh, A., 1922. The Anatomy and Physiology of Capillaries. Yale University Press, New Haven, Conn.

Kruggel, F., Turner, J., Muftuler, L.T., Alzheimer's Disease Neuroimaging, 2010. Impact of scanner hardware and imaging protocol on image quality and compartment volume precision in the ADNI cohort. NeuroImage 49, 2123–2133.

Lawrence, K.S., Owen, D., Wang, D.J.J., 2012. A two-stage approach for measuring

vascular water exchange and arterial transit time by diffusion-weighted perfusion MRI. Magn. Reson. Med. 67, 1275–1284.
Le Bihan, D., 1992. Theoretical principles of perfusion imaging. Application to magnetic resonance imaging. Investig. Radiol. 27 (Suppl. 2), S6–11.
Le Bihan, D., 2017. What can we see with IVIM MRI? NeuroImage 1–12.
Le Bihan, D., Turner, R., 1992. The capillary network: a link between IVIM and classical perfusion. Magn. Reson. Med. 27, 171–178.
Le Bihan, D., Breton, E., Lallemand, D., Grenier, P., Cabanis, E., Laval-Jeantet, M., 1986. MR imaging of intravoxel incoherent motions: application to diffusion and perfusion in neurologic disorders. Radiology 161, 401–407.
Le Bihan, D., Breton, E., Lallemand, D., Aubin, M.L., Vignaud, J., Laval-Jeantet, M., 1988. Separation of diffusion and perfusion in intravoxel incoherent motion MR imaging. Radiology 168, 497–505.
Lemke, A., Stieltjes, B., Schad, L.R., Laun, F.B., 2011. Toward an optimal distribution of b values for intravoxel incoherent motion imaging. Magn. Reson. Imaging 29, 766–776.
Li, K.L., Zhu, X., Hylton, N., Jahng, G.H., Weiner, M.W., Schuff, N., 2005. Four-phase single-capillary stepwise model for kinetics in arterial spin labeling MRI. Magn. Reson. Med. 53, 511–518.
Li, Y.T., Cercueil, J.P., Yuan, J., Chen, W., Loffroy, R., Wang, Y.X., 2017. Liver intravoxel incoherent motion (IVIM) magnetic resonance imaging: a comprehensive review of published data on normal values and applications for fibrosis and tumor evaluation. Quant. Imaging Med. Surg. 7, 59–78.
Liang, L., Chen, W.B., Chan, K.W., Li, Y.G., Zhang, B., Liang, C.H., Liu, G.S., Zhang, S.X., 2016. Using intravoxel incoherent motion MR imaging to study the renal pathophysiological process of contrast-induced acute kidney injury in rats: Comparison with conventional DWI and arterial spin labelling. Eur. Radiol. 26, 1597–1605.
Louis, D.N., Perry, A., Reifenberger, G., von Deimling, A., Figarella-Branger, D., Cavenee, W.K., Ohgaki, H., Wiestler, O.D., Kleihues, P., Ellison, D.W., 2016. The 2016 World Health Organization classification of tumors of the central nervous system: a summary. Acta Neuropathol. 131, 803–820.
Luciani, A., Vignaud, A., Cavet, M., Nhieu, J.T., Mallat, A., Ruel, L., Laurent, A., Deux, J.F., Brugieres, P., Rahmouni, A., 2008. Liver cirrhosis: intravoxel incoherent motion MR imaging–pilot study. Radiology 249, 891–899.
MacIntosh, B.J., Filippini, N., Chappell, M.A., Woolrich, M.W., MacKay, C.E., Jezzard, P., 2010. Assessment of arterial arrival times derived from multiple inversion time pulsed arterial spin labeling MRI. Magn. Reson. Med. 63, 641–647.
Markus, H.S., Lythgoe, D.J., Ostegaard, L., O'Sullivan, M., Williams, S.C.R., 2000. Reduced cerebral blood flow in white matter in ischaemic leukoaraiosis demonstrated using quantitative exogenous contrast based perfusion MRI. J. Neurol. Neurosurg. Psych. 69, 48–53.
Marzi, S., Forina, C., Marucci, L., Giovinazzo, G., Giordano, C., Piludu, F., Landoni, V., Spriano, G., Vidiri, A., 2015. Early radiation-induced changes evaluated by intravoxel incoherent motion in the major salivary glands. J. Magn. Reson. Imaging 41, 974–982.
Meeus, E.M., Novak, J., Dehghani, H., Peet, A.C., 2018. Rapid measurement of intravoxel incoherent motion (IVIM) derived perfusion fraction for clinical magnetic resonance imaging. MAGMA 31, 269–283.
Muir, K.W., Buchan, A., von Kummer, R., Rother, J., Baron, J.C., 2006. Imaging of acute stroke. Lancet Neurol. 5, 755–768.
Mullen, K.M., Huang, R.Y., 2017. An update on the approach to the imaging of brain tumors. Curr. Neurol. Neurosci. Rep. 17, 53.
Neil, J.J., Ackerman, J.J.H., 1992. Detection of pseudodiffusion in rat-brain following blood substitution with perfluorocarbon. J. Magn. Reson. 97, 194–201.
Neil, J.J., Scherrer, L.A., Ackerman, J.J.H., 1991. An approach to solving the dynamic-range problem in measurement of the pseudodiffusion coefficient invivo with spin echoes. J. Magn. Reson. 95, 607–614.
Neil, J.J., Bosch, C.S., Ackerman, J.J.H., 1994. An evaluation of the sensitivity of the intravoxel incoherent motion (Ivim) method of blood-flow measurement to changes in cerebral blood-flow. Magn. Reson. Med. 32, 60–65.
Obrig, H., 2014. NIRS in clinical neurology - a 'promising' tool? Neuroimage 85, 535–546.
O'Sullivan, M., Lythgoe, D.J., Pereira, A.C., Summers, P.E., Jarosz, J.M., Williams, S.C.R., Markus, H.S., 2002. Patterns of cerebral blood flow reduction in patients with ischemic leukoaraiosis. Neurology 59, 321–326.
Paldino, M.J., Barboriak, D.P., 2009. Fundamentals of quantitative dynamic contrast-enhanced MR imaging. Magn. Reson. Imaging Clin. N. Am. 17, 277–289.
Parkes, L.M., Tofts, P.S., 2002. Improved accuracy of human cerebral blood perfusion measurements using arterial spin labeling: accounting for capillary water permeability. Magn. Reson. Med. 48, 27–41.
Plate, K.H., Breier, G., Weich, H.A., Risau, W., 1992. Vascular endothelial growth factor is a potential tumour angiogenesis factor in human gliomas in vivo. Nature 359, 845–848.
Pullicino, R., Radon, M., Biswas, S., Bhojak, M., Das, K., 2018. A review of the current evidence on gadolinium deposition in the brain. Clin. Neuroradiol. 28, 159–169.
Rahatli, F.K., Donmez, F.Y., Kibaroglu, S., Kesim, C., Haberal, K.M., Turnaoglu, H., Agildere, A.M., 2018. Does renal function affect gadolinium deposition in the brain? Eur. J. Radiol. 104, 33–37.
Reig, S., Sanchez-Gonzalez, J., Arango, C., Castro, J., Gonzalez-Pinto, A., Ortuno, F., Crespo-Facorro, B., Bargallo, N., Desco, M., 2009. Assessment of the increase in variability when combining volumetric data from different scanners. Hum. Brain Mapp. 30, 355–368.
Roob, G., Schmidt, R., Kapeller, P., Lechner, A., Hartung, H.P., Fazekas, F., 1999. MRI evidence of past cerebral microbleeds in a healthy elderly population. Neurology 52, 991–994.
Schnack, H.G., van Haren, N.E., Hulshoff Pol, H.E., Picchioni, M., Weisbrod, M., Sauer, H., Cannon, T., Huttunen, M., Murray, R., Kahn, R.S., 2004. Reliability of brain volumes from multicenter MRI acquisition: a calibration study. Hum. Brain Mapp. 22, 312–320.
Shim, W.H., Kim, H.S., Choi, C.G., Kim, S.J., 2015. Comparison of apparent diffusion coefficient and intravoxel incoherent motion for differentiating among glioblastoma, metastasis, and lymphoma focusing on diffusion-related parameter. PLoS One 10.
Sourbron, S.P., Buckley, D.L., 2013a. Classic models for dynamic contrast-enhanced MRI. NMR Biomed. 26, 1004–1027.
Sourbron, S.P., Buckley, D.L., 2013b. Classic models for dynamic contrast-enhanced MRI. NMR Biomed. 26, 1004–1027.
Stejskal, E.O., Tanner, J.E., 1965. Spin diffusion measurements: spin echoes in the presence of a time-dependent field gradient. J. Chem. Phys. 42, 288.
Suh, C.H., Kim, H.S., Lee, S.S., Kim, N., Yoon, H.M., Choi, C.G., Kim, S.J., 2014. Atypical imaging features of primary central nervous system lymphoma that mimics glioblastoma: utility of intravoxel incoherent motion MR imaging. Radiology 272, 504–513.
Suo, S., Cao, M., Zhu, W., Li, L., Li, J., Shen, F., Zu, J., Zhou, Z., Zhuang, Z., Qu, J., Chen, Z., Xu, J., 2016. Stroke assessment with intravoxel incoherent motion diffusion-weighted MRI. NMR Biomed. 29, 320–328.
Tanner, J.E., Stejskal, E.O., 1968. Restricted self-diffusion of protons in colloidal systems by pulsed-gradient spin-echo method. J. Chem. Phys. 49, 1768.
Togao, O., Hiwatashi, A., Yamashita, K., Kikuchi, K., Mizoguchi, M., Yoshimoto, K., Suzuki, S.O., Iwaki, T., Obara, M., Van Cauteren, M., Honda, H., 2016. Differentiation of high-grade and low-grade diffuse gliomas by intravoxel incoherent motion MR imaging. Neuro-Oncology 18, 132–141.
Toh, C.H., Castillo, M., Wong, A.M., Wei, K.C., Wong, H.F., Ng, S.H., Wan, Y.L., 2008. Primary cerebral lymphoma and glioblastoma multiforme: differences in diffusion characteristics evaluated with diffusion tensor imaging. AJNR Am. J. Neuroradiol. 29, 471–475.
Wang, J.J., Fernandez-Seara, M.A., Wang, S.M., St Lawrence, K.S., 2007. When perfusion meets diffusion: in vivo measurement of water permeability in human brain. J. Cereb. Blood Flow Metab. 27, 839–849.
Wardlaw, J.M., 2010. Blood-brain barrier and cerebral small vessel disease. J. Neurol. Sci. 299, 66–71.
Wardlaw, J.M., Doubal, F.N., Valdes-Hernandez, M., Wang, X., Chappell, F.M., Shuler, K., Armitage, P.A., Carpenter, T.C., Dennis, M.S., 2013a. Blood-brain barrier permeability and long-term clinical and imaging outcomes in cerebral small vessel disease. Stroke 44, 525–527.
Wardlaw, J.M., Smith, C., Dichgans, M., 2013b. Mechanisms of sporadic cerebral small vessel disease: insights from neuroimaging. Lancet Neurol. 12, 483–497.
Wardlaw, J.M., Smith, E.E., Biessels, G.J., Cordonnier, C., Fazekas, F., Frayne, R., Lindley, R.I., O'Brien, J.T., Barkhof, F., Benavente, O.R., Black, S.E., Brayne, C., Breteler, M., Chabriat, H., Decarli, C., de Leeuw, F.E., Doubal, F., Duering, M., Fox, N.C., Greenberg, S., Hachinski, V., Kilimann, I., Mok, V., Oostenbrugge, R., Pantoni, L., Speck, O., Stephan, B.C., Teipel, S., Viswanathan, A., Werring, D., Chen, C., Smith, C., van Buchem, M., Norrving, B., Gorelick, P.B., Dichgans, M., Neuroimaging, S.T.f.R.V.c.o., 2013c. Neuroimaging standards for research into small vessel disease and its contribution to ageing and neurodegeneration. Lancet Neurol. 12, 822–838.
Williams, D.S., Detre, J.A., Leigh, J.S., Koretsky, A.P., 1992. Magnetic resonance imaging of perfusion using spin inversion of arterial water. Proc. Natl. Acad. Sci. U S A 89, 212–216.
Wintermark, M., Sesay, M., Barbier, E., Borbely, K., Dillon, W.P., Eastwood, J.D., Glenn, T.C., Grandin, C.B., Pedraza, S., Soustiel, J.F., Nariai, T., Zaharchuk, G., Caille, J.M., Dousset, V., Yonas, H., 2005. Comparative overview of brain perfusion imaging techniques. J. Neuroradiol. 32, 294–314.
Wirestam, R., Brockstedt, S., Lindgren, A., Geijer, B., Thomsen, C., Holtas, S., Stahlberg, F., 1997. The perfusion fraction in volunteers and in patients with ischaemic stroke. Acta Radiol. 38, 961–964.
Wonderlick, J.S., Ziegler, D.A., Hosseini-Varnamkhasti, P., Locascio, J.J., Bakkour, A., van der Kouwe, A., Triantafyllou, C., Corkin, S., Dickerson, B.C., 2009. Reliability of MRI-derived cortical and subcortical morphometric measures: effects of pulse sequence, voxel geometry, and parallel imaging. NeuroImage 44, 1324–1333.
Wong, S.M., Zhang, C.E., van Bussel, F.C.G., Staals, J., Jeukens, C.R.L.P.N., Hofman, P.A.M., van Oostenbrugge, R.J., Backes, W.H., Jansen, J.F.A., 2017. Simultaneous investigation of microvasculature and parenchyma in cerebral small vessel disease using intravoxel incoherent motion imaging. Neuroimage Clin. 14, 216–221.
World Health Organization, 2017. The Top 10 Causes of Death.
Wu, W.C., Chen, Y.F., Tseng, H.M., Yang, S.C., My, P.C., 2015. Caveat of measuring perfusion indexes using intravoxel incoherent motion magnetic resonance imaging in the human brain. Eur. Radiol. 25, 2485–2492.
Yamada, I., Aung, W., Himeno, Y., Nakagawa, T., Shibuya, H., 1999. Diffusion coefficients in abdominal organs and hepatic lesions: evaluation with intravoxel incoherent motion echo-planar MR imaging. Radiology 210, 617–623.
Yamasaki, F., Kurisu, K., Satoh, K., Arita, K., Sugiyama, K., Ohtaki, M., Takaba, J., Tominaga, A., Hanaya, R., Yoshioka, H., Hama, S., Ito, Y., Kajiwara, Y., Yahara, K., Saito, T., Thohar, M.A., 2005. Apparent diffusion coefficient of human brain tumors at MR imaging. Radiology 235, 985–991.
Yamashita, K., Hiwatashi, A., Togao, O., Kikuchi, K., Kitamura, Y., Mizoguchi, M., Yoshimoto, K., Kuga, D., Suzuki, S.O., Baba, S., Isoda, T., Iwaki, T., Iihara, K., Honda, H., 2016. Diagnostic utility of intravoxel incoherent motion mr imaging in differentiating primary central nervous system lymphoma from glioblastoma multiforme. J. Magn. Reson. Imaging 44, 1256–1261.
Yang, S.H., Lin, J., Lu, F., Han, Z.H., Fu, C.X., Lv, P., Liu, H., Gao, D.M., 2017. Evaluation of antiangiogenic and antiproliferative effects of sorafenib by sequential histology and intravoxel incoherent motion diffusion-weighted imaging in an orthotopic hepatocellular carcinoma xenograft model. J. Magn. Reson. Imaging 45, 270–280.
Yao, Y., Zhang, S., Tang, X., Zhang, S., Shi, J., Zhu, W., Zhu, W., 2016. Intravoxel incoherent motion diffusion-weighted imaging in stroke patients: initial clinical

experience. Clin. Radiol. 71 (938), e911–e936.
Zhang, S.X., Yao, Y.H., Zhang, S., Zhu, W.J., Tang, X.Y., Qin, Y.Y., Zhao, L.Y., Liu, C.X., Zhu, W.Z., 2015. Comparative study of DSC-PWI and 3D-ASL in ischemic stroke patients. J. Huazhong Univ. Sci. Technol. Med. Sci. 35, 923–927.
Zhang, X., Ingo, C., Teeuwisse, W.M., Chen, Z., van Osch, M.J.P., 2018. Comparison of perfusion signal acquired by arterial spin labeling-prepared intravoxel incoherent motion (IVIM) MRI and conventional IVIM MRI to unravel the origin of the IVIM signal. Magn. Reson. Med. 79, 723–729.
Zhou, J., Wilson, D.A., Ulatowski, J.A., Traystman, R.J., van Zijl, P.C., 2001. Two-compartment exchange model for perfusion quantification using arterial spin tagging. J. Cereb. Blood Flow Metab. 21, 440–455.